Multipole edge plasma modes of parabolic quantum wells

1996 J. Phys.: Condens. Matter 8 9037

(http://iopscience.iop.org/0953-8984/8/46/009)

J. Phys.: Condens. Matter **8** (1996) 9037–9048. Printed in the UK

Multipole edge plasma modes of parabolic quantum wells

Q Guo, Y P Feng, H C Poon and C K Ong

Department of Physics, National University of Singapore, Kent Ridge, Singapore 119260

Received 16 May 1996, in final form 4 August 1996

Abstract. We study the excitation modes in parabolic quantum wells via an approach based on the invariant-imbedding method in the random-phase approximation. For large values of wave vectors, several higher-multipole edge plasmon modes have been observed for the first time below the intrasubband plasmon in parabolic quantum wells in addition to the normal surface plasmon modes. It is shown that the edge electron density profile has an important effect on the higher-multipole edge plasmon modes.

1. Introduction

In recent years, there has been increasing interest in the investigation of electron systems of wide remotely doped parabolic quantum wells (PQW) [1–4] both experimentally and theoretically; the main reason for this is that parabolic quantum wells are structures that behave like uniform-density electron slabs. This grows out of attempts to realize the theoretical construction of jellium, consisting of a highly mobile dilute electron gas in the potential of a positively charged background. The excitation modes play a significant role in the transport and optical properties in these electron gas systems, and have received considerable attention recently [5–13]. Two collective modes were experimentally observed in the far-infrared (FIR) transmission spectra of PQW and had been identified as the normal surface plasmons [5]. The low-frequency mode is called an intrasubband plasmon, the excited resonant oscillation of the quantum well in the 2D plane (the x–y plane), while the high-frequency mode is called an intersubband plasmon, which evolves out of transitions between adjacent bound levels in the well which correspond to oscillations of the electrons perpendicular to the interface (the z-direction). Kaloudis *et al* [6] studied the resonant coupling of collective intra- and intersubband excitations in a parabolically confined electron system. The dimensional resonances have been directly observed by use of a grating-coupler technique [7]. Recently, Liao *et al* [8] studied the dispersion and magnetic field dependence of both inter-Landau-level and intersubband magnetoplasma modes in a wide parabolic quantum well by inelastic light scattering. Brey *et al* [9] theoretically demonstrated that an electron gas in an ideal parabolic quantum well absorbs light only at the bare harmonic oscillator frequency. Calculations within the time-dependent local density approximation (TDLDA) and the random-phase approximation (RPA) yielded an excitation spectrum with two major peaks for a small wave vector and for frequencies up to the bulk plasma frequency [10–13]. The locations of these relatively strong peaks are consistent with experimental observations and also agree well with the theoretical predictions for the plasma modes of a uniform slab of Drude electrons. Recently, Xia and Quinn [14] studied the resonant modes below the 2D bulk plasmon for 2D electron gas with a non-abrupt edge density profile

0953-8984/96/469037+12$19.50

using a simple optical model. However, as far as we know, there has been no investigation of the corresponding resonant modes below the intrasubband plasmon in the quantum well using the RPA. In the present work, we will study the excitation spectra of PQW with large values of wave vectors via an approach based on the invariant-imbedding method [10]. In contrast to the case for previous calculations, several weak resonant modes below the 2D intrasubband frequency are observed in the excitation spectra with large wave vectors, and these resonant modes will be explored in our calculation.

In the following section, we will outline the numerical method based on the invariant-imbedding method. In section 3, we will discuss the origins and properties of the weak excitation modes appearing below the intrasubband plasma mode. Finally we will summarize our results in section 4.

2. The numerical method

For $Ga_{1-x}Al_xAs$ quantum wells, the effective mass m^* is about $0.067m_0$ and the dielectric constant ε_0 is around 13.0, which give an effective Bohr radius a_0 of approximately 100 Å in such materials. Since the effective Bohr radius is much larger than the lattice constant, we can ignore the crystalline structure of the host, and treat the conduction band edge E_c of the quantum well as an external potential energy, confining the motion of the electrons in the conduction band, on the basis of the envelope function approximation [15]. According to Poisson's law, the external potential of a quantum well can be mimicked as the potential due to the background positive charge n^+ in a slab. In the calculation, such fictitious positive charge density n^+ is used to parametrize the parabolic quantum well. For a given PQW with n^+ and N_s, the total number of electrons per unit area, the approximate width $L = N_s/n^+$ that the electrons occupy is taken to be the width of the quantum well. Within the constant-effective-mass approximation, the self-consistent Kohn–Sham eigenfunction may be written as

$$\Psi_J \equiv \Psi_{k_\parallel, j}(\boldsymbol{r}) = \frac{1}{2\pi} \exp(\mathrm{i}\boldsymbol{k} \cdot \boldsymbol{\rho})\psi_j(z) \tag{1}$$

with eigenenergy

$$E_J \equiv E(\boldsymbol{k}_\parallel, j) = \varepsilon_j + \frac{1}{2}k_\parallel^2 \tag{2}$$

where $\boldsymbol{r}$ is a position vector, and $\boldsymbol{\rho}$ and z are the projections of $\boldsymbol{r}$ parallel and normal to the well respectively, while $\boldsymbol{k}_\parallel$ is the projection of $\boldsymbol{k}$ parallel to the well. ε_j is the eigenenergy of the one-dimensional Schrödinger equation with a self-consistent potential, and $\psi_j(z)$ is the corresponding eigenfunction. The self-consistent electronic structures of quantum wells are calculated via an approach based on the invariant-imbedding method.

For independent electrons moving in the self-consistent ground-state potential, the density response δn_f to a small time-dependent external perturbation

$$\delta v = v_x(z, q_\parallel) \exp\left[\mathrm{i}(\boldsymbol{q}_\parallel \cdot \boldsymbol{r} - \omega t)\right] \tag{3}$$

can be written as

$$\delta n_f(z, q_\parallel, \omega) = \int \mathrm{d}z' \ \Pi^0(q_\parallel, z, z', \omega) v_x(z', q_\parallel) \tag{4}$$

where the free-response function is given by

$$\Pi^0(q_\parallel, z, z', \omega) = \frac{1}{2\pi^2} \sum_i^{occ} \psi_i(z)\psi_i(z') \int \mathrm{d}\boldsymbol{k}_\parallel \left\{ \sum_j \frac{\psi_j(z)\psi_j(z')}{\varepsilon^+ - \varepsilon_j} + \sum_j \frac{\psi_j(z)\psi_j(z')}{\varepsilon^- - \varepsilon_j} \right\} \tag{5}$$

where

$$\varepsilon^{\pm} = \varepsilon_i \pm (\omega + \boldsymbol{k}_{\parallel} \cdot \boldsymbol{q}_{\parallel}) - \frac{1}{2} q_{\parallel}^2. \tag{6}$$

It is noted that the two terms in the braces of equation (5) are just the Green's functions for the one-dimensional Schrödinger equation with energies of ε^+ and ε^- respectively. Therefore the free-response function can be written as

$$\Pi^0(q_{\parallel}, z, z', \omega) = \frac{1}{2\pi^2} \sum_i^{occ} \psi_i(z)\psi_i(z') \int \mathrm{d}\boldsymbol{k}_{\parallel} \left[G^+(z, z', \varepsilon^+) + G^+(z, z', \varepsilon^-) \right]. \tag{7}$$

For the calculation of the free-response function, we choose the x-axis such that k_x is parallel to $\boldsymbol{q}_{\parallel}$. So equation (7) can be rewritten as

$$\Pi^0(q_{\parallel}, z, z', \omega) = \frac{1}{\pi^2} \sum_i^{occ} \psi_i(z)\psi_i(z') \int_{-k_i}^{k_i} \mathrm{d}k_x \sqrt{k_i^2 - k_x^2} \left[G^+(z, z', \varepsilon^+) + G^+(z, z', \varepsilon^-) \right] \tag{8}$$

where

$$k_i = \sqrt{2(\varepsilon_f - \varepsilon_i)} \tag{9}$$

$$\varepsilon^{\pm} = \varepsilon_i \pm (\omega + k_x q_{\parallel}) - \frac{1}{2} q_{\parallel}^2. \tag{10}$$

The above function is evaluated on a discrete grid of z- and z'-points. In order to produce numerically tractable results, a small imaginary part of 0.002 au* (starred Hartree units; see below) has been added to ω, the frequency of the external field. Since the free-response function has a cusp at $z' = z$, the z'-integral will be split into two separate parts at $z' = z$, and the integration over z' is done by Gaussian quadrature. The Green's functions are obtained by the invariant-imbedding method [10]. The integration of the Green's function $G^+(z, z', \varepsilon^+)$ along the real axis in the k_x-plane from $-k_i$ to k_i is deformed to a semicircle in the upper complex half-plane. Because the Green's functions are much smoother functions of k_x along such an integral path than along the real axis, only a few points need to be sampled in the integration. In contrast, $G^+(z, z', \varepsilon^-)$ is analytic in the lower complex half-plane. Using the basic property of Green's functions

$$G^*(z, z', \varepsilon) = G(z, z', \varepsilon^*) \tag{11}$$

we compute the Green's function $G^+(z, z', \varepsilon^-)$ in the same way as $G^+(z, z', \varepsilon^+)$.

Similar to equation (4), the RPA density response function is defined as

$$\delta n_{RPA}(z, q_{\parallel}, \omega) = \int \mathrm{d}z' \; \Pi^{RPA}(q_{\parallel}, z, z', \omega) v(z', q_{\parallel}). \tag{12}$$

It can be proved that the RPA response function is related to the free-response function by the integral equation

$$\Pi^{RPA}(z, z', \boldsymbol{q}_{\parallel}, \omega) = \Pi^0(z, z', \boldsymbol{q}_{\parallel}, \omega) + \int\int \mathrm{d}z_1 \; \mathrm{d}z_2 \; \Pi^0(z, z_1, \boldsymbol{q}_{\parallel}, \omega) v(z_1, z_2) \Pi^{RPA}(z_2, z', \boldsymbol{q}_{\parallel}, \omega) \tag{13}$$

where

$$v(z_1, z_2) = \frac{\partial^2}{\partial n^2}(n\varepsilon_{xc})\delta(z_1 - z_2) + \frac{2\pi}{q_{\parallel}} \exp(-q_{\parallel}|z_1 - z_2|) \tag{14}$$

is the function describing the dependence of the potential field on the electron density for a quantum well. ε_{xc} is the exchange–correlation kernel. Ignoring frequency dependence, ε_{xc} is chosen to be the simple Wigner form [16] for both the ground state and the excited state:

$$\varepsilon_{xc} = -\frac{0.458}{r_s} - \frac{0.44}{r_s + 7.8} \tag{15}$$

where

$$r_s \equiv r_s(z) = \left[\frac{4}{3}\pi n(z)\right]^{-1/3}. \tag{16}$$

$n(z)$ is the self-consistent electron density. The RPA response function is calculated by solving the matrix equation (13).

In order to simulate spatially non-uniform excitation of a quantum well, the external perturbation potential is chosen to be

$$v_x(z, q_\parallel) = \exp(q_\parallel z). \tag{17}$$

So the strength function can be calculated from

$$M(q_\parallel, \omega) = -\mathrm{Im} \int\int \mathrm{d}z\ \mathrm{d}z'\ \exp(q_\parallel z)\Pi^{RPA}(z, z', q_\parallel, \omega)\exp(q_\parallel z'). \tag{18}$$

This strength function can be directly obtained from experimental measurements. The same function appears in the dipole theory of electron energy loss [17] as well as the theory of infrared (IR) absorption aided by a grating coupler [18, 19].

In the $Ga_{1-x}Al_xAs$ system, the effective mass m^* and dielectric constant ε vary according to [20]

$$m^*(x)/m_0 = 0.067 + 0.0838x \tag{19}$$

and

$$\varepsilon(x) = 13.18 - 3.12x \tag{20}$$

respectively, where m_0 is the mass of an electron. In our calculation, the effective mass m^* and dielectric constant ε have been taken to be constants: $m^* = 0.067$, and $\varepsilon = 12.9$. For convenience, we use 'starred Hartree units', au*, in which $e^2/\varepsilon = 1$, $m^* = 1$, $\hbar = 1$. So 1 au* of length is equal to 102 Å, 1 au* of energy is 11 meV, which is equivalent to a photon with the reciprocal wavelength 88.5 cm^{-1}.

3. Results and discussion

We start with a parabolic quantum well (PQW) of width $L = 8.8$ au* and density $n^+ = 0.0275$ au*. The excitation spectrum with a small wave vector of $q_\parallel = 0.016$ au* is shown in figure 1. Two peaks appear in the spectrum for a very wide range of frequencies. They are the normal surface plasma modes, i.e. the intersubband plasma mode and the intrasubband plasma mode. The positions of these peaks are in good agreement with the experimental data [5]. The resonant frequencies of the excitation modes in PQW can also be estimated via a non-retarded, local optical model of a uniform slab of Drude electrons. In this model, the dielectric function within a slab of thickness d can be written as

$$\varepsilon = \varepsilon_0(1 - \omega_p^2/\omega^2) \tag{21}$$

where

$$\omega_p^2 = 4\pi n \tag{22}$$

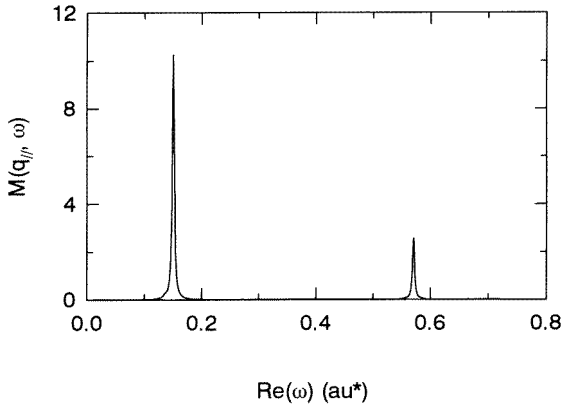

Figure 1. Excitation spectra for PQW with width $d = 8.8$ au*, density $n^+ = 0.0275$ au*, $q_\parallel = 0.016$ au*, and $\mathrm{Im}(\omega) = 0.002$ au*.

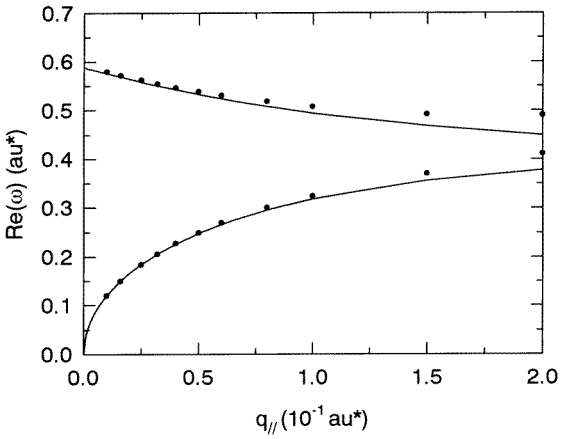

Figure 2. A comparison of the dispersion relations of RPA calculations (dots) and those from the local optical model (solid lines) for the intersubband plasmon modes (upper) and the intrasubband plasmon modes (lower) with width $L = 8.8$ au* and densities $n^+ = 0.0275$ au*.

is the bulk plasma frequency, and n is the electron density of the slab. Assuming a spatially local response and neglecting incoherent scattering, the dispersions of the two normal plasma modes are given by

$$\omega_\pm^2 = \frac{1}{2}\omega_p^2(1 \pm \exp(q_\parallel d)). \tag{23}$$

In figure 2, we compare the dispersion relations of the normal plasma modes calculated within the RPA with those from equation (23). It can be seen that the simple local optical model describes the positions of the resonant modes quite well for small $q_\parallel$. However, it underestimates the excitation frequency for large $q_\parallel$.

In the following, we will consider the excitation modes in parabolic quantum wells with large wave vectors.

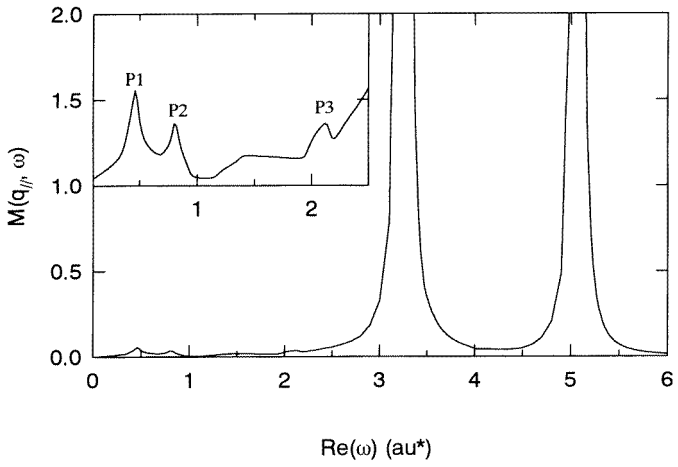

Figure 3. Excitation spectra for PQW with width $L = 8.8$ au*, density $n^+ = 0.0275$ au*, $q_\parallel = 0.10$ au*, and $\mathrm{Im}(\omega) = 0.002$ au*. The inset shows the three weak resonant peaks P1, P2 and P3 below the intrasubband plasmon mode.

3.1. The excitation spectrum for large wave vectors

In figure 3, we report the calculated excitation spectra of PQW with width $L = 8.8$ au* and density $n^+ = 0.0275$ au* for a large value of the wave vector $q_\parallel = 0.10$ au*. In addition to the normal surface plasmon modes, three weaker peaks P1, P2, P3 appear below the intrasubband mode. These modes are located at frequencies of 0.046 au*, 0.081 au* and 0.212 au* respectively. To explore their physical origins, we calculate the induced density profile, which is defined as

$$\Delta n(z) = \frac{\partial^2(\delta n(z))}{\partial(\mathrm{Re}(\omega))^2}. \tag{24}$$

$\Delta n(z)$ is used instead of $\delta n(z)$ because the response $\delta n(z)$ to the external field will be richest in the induced density profile when $\mathrm{Re}(\omega)$ is at resonance, and resonant peaks show up more clearly in the above definition for weak resonances, and non-resonant baselines are approximately filtered out by the second frequency derivative, while $\delta n(z)$ is dominated by the eigenfunction for strong resonances. Shown in figure 4 are the induced density profiles of the three peaks. We first analyse the peaks P2 and P3. The induced density profile of P3 in figure 4(c) is identical to that of the excitation mode observed in neutral quantum wells [10–12], which was identified as a multipole plasma mode. The multipole plasma mode was predicted theoretically on simple surfaces [21, 22] and first observed experimentally by Tsuei *et al* [23] on K and Na surfaces. Schaich and Dobson [13] suggested that the intersubband transition from the first subband to the fourth subband is also another reasonable interpretation for that excitation mode. If one compares the values of $\Delta\varepsilon_{1,4} = E_4 - E_1 = 0.538$ au* with the frequency of P3, it is clear that this interpretation is unreasonable. The intersubband transition picture obviously also fails to explain excitation mode P2, because there are three subband energies below the Fermi energy level and the induced density profile of any intersubband transition is more complex than that of peak P2. It is interesting to note that peaks P2 and P3 have very special properties. The induced density profile P2 is an even function of z, while that of P3 is an odd function of z. Since

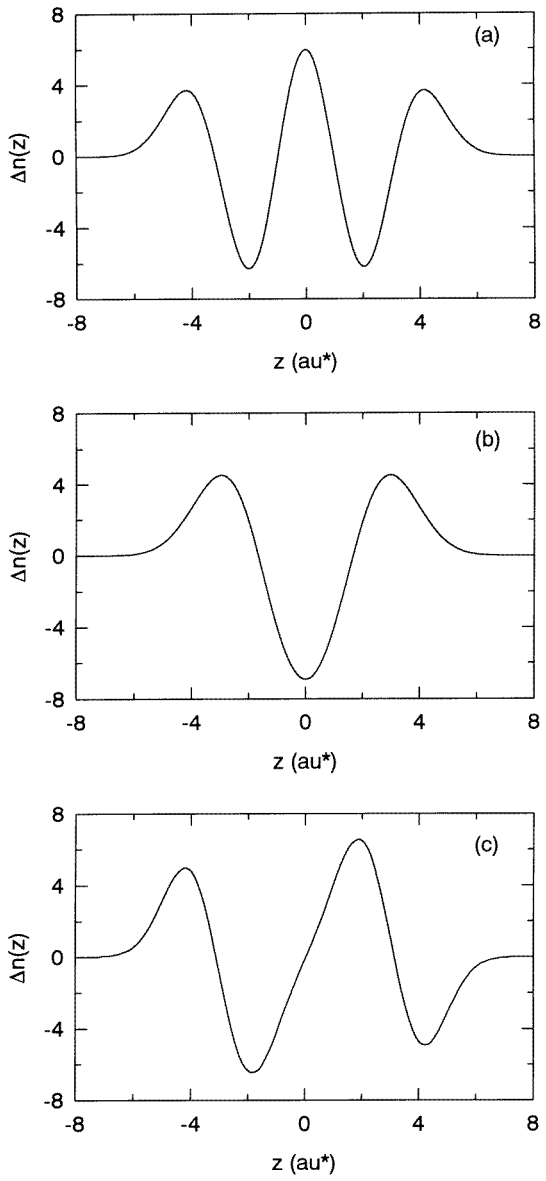

Figure 4. Induced density profiles at the frequencies of the three peaks (a) P1, (b) P2 and (c) P3 in the excitation spectra of figure 3.

they are located below the intrasubband plasmon mode, we associate peaks P2 and P3 with higher-multipole edge plasmon modes.

The higher-multipole plasmon modes are so named since, unlike the normal surface plasmons, the integrals of their induced densities with respect to each surface are nearly zero. The higher-multipole edge plasmon modes are essentially bulk 2D plasmons of the low-electron-density surface region [24]. Regular edge plasmons were first studied by Mast *et al* [25], and by Glattli *et al* [26]. The regular magnetoplasma edge modes of two-

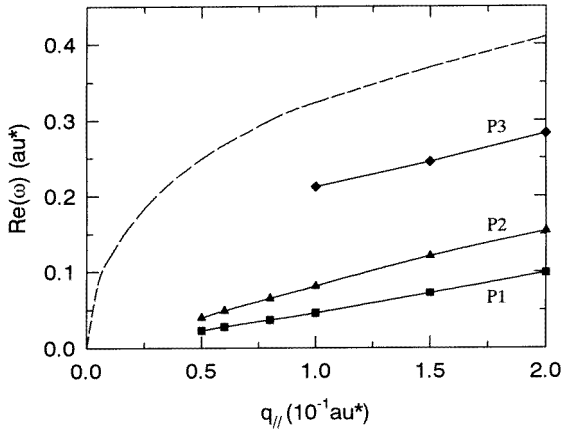

Figure 5. The dispersion relation Re(ω) versus $q_\parallel$ for the higher-multipole edge plasmon modes P1, P2 , P3 and the intrasubband plasmon mode (dashed line) in the excitation spectrum in figure 3.

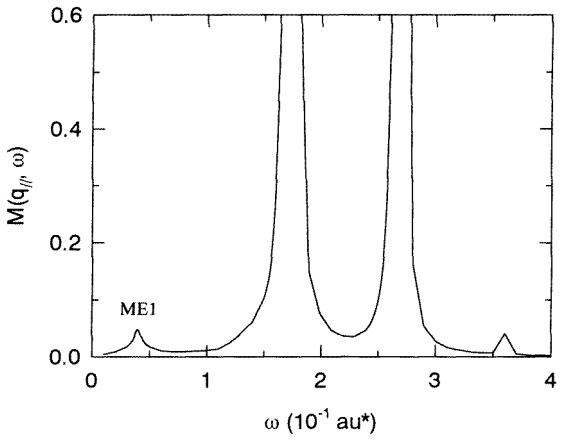

Figure 6. Excitation spectra for PQW with width $L = 8.8$ au*, density $n^+ = 0.0075$ au*, $q_\parallel = 0.10$ au*, and Im(ω) $= 0.002$ au*.

dimensional electron gas (2DEG) were investigated by Wu *et al* [27, 28]. Recently, Xia and Quinn [14] investigated the higher-multipole edge modes of a 2DEG with a non-abrupt edge density profile using a simple optical model. They found a sequence of higher-multipole edge modes, which exist as well-defined edge excitations at finite values of $q_\parallel$. Necessary conditions for the existence of higher-multipole modes include both a spatially varying electron density and dispersion of the bulk plasmon [24]. For a three-dimensional electron gas a non-local conductivity is required for dispersion of the bulk plasmon. In contrast, for a 2DEG the bulk plasmon frequency depends on the wave vector even in a simple local theory of conduction. In the parabolic quantum well, the quantum effect causes the electrons in the well to spread outside the well and form an electron gas with an edge density profile. So it is reasonable that higher-multipole edge plasmon modes appear in the excitation spectra

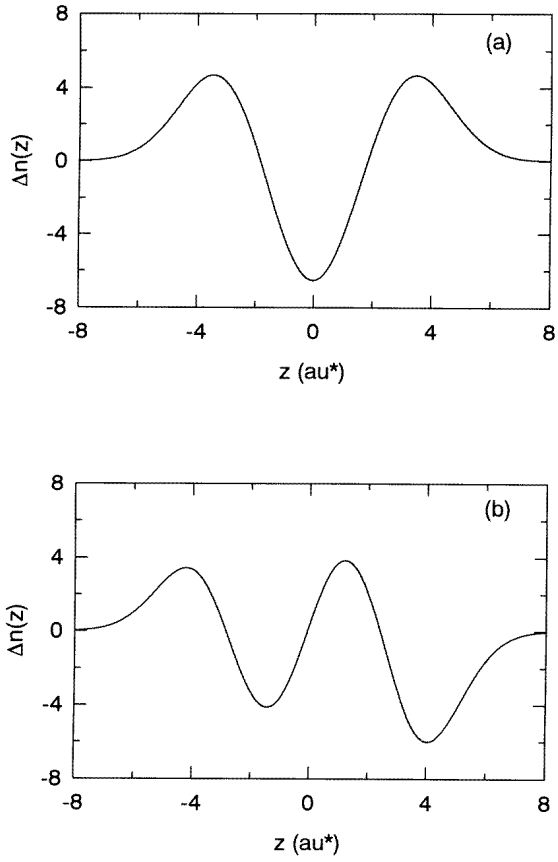

Figure 7. Induced density profiles of (a) the even higher-multipole edge plasmon mode ME1 and (b) the corresponding odd mode MO1 below the intrasubband plasmon in the excitation spectra of PQW with width $L = 8.8$ au*, $n^+ = 0.0075$ au*.

of PQW. It is expected that there are more interesting features in the edge plasmon modes for narrow quantum wells due to the symmetric environment on both sides of the quantum well. The edge plasmons will appear in the edge regions of both surfaces and the symmetry on both sides of the quantum well causes the frequencies of the edge plasmon modes to be same on both sides, so in the case of a narrow quantum well, the electromagnetic fields of the two surfaces interact and the frequency splits into two modes: a high-frequency mode whose induced electron density is asymmetric with respect to the plane $z = 0$ and a low-frequency mode whose induced electron density is symmetric with respect to the plane $z = 0$. Resonant modes P2 and P3 are a case in point. Taking into account that they have another interesting characteristic, i.e. their induced density profiles integrate to nearly zero with respect to each surface separately, we can identify them as being even and odd higher-multipole edge plasmon modes respectively. The induced density profile of peak P1 is an even function of z, and is located below the even edge plasmon mode P2. So we can identify P1 as another even higher-multipole edge plasmon mode.

In figure 5, we present the dispersion profiles of peaks P1, P2, P3 and the intrasubband plasmon as well. It is noted that two even edge plasmon modes P1 and P2 emerge first at

a small value of $q_{\parallel}$, while the first odd edge plasmon mode P3 corresponding to the even edge plasmon mode P2 appears at $q_{\parallel} \cong 0.10$ au*. However, we have not observed the corresponding odd edge plasmon mode P1 even when we increase $q_{\parallel}$ up to 0.20 au*. It is also noted that these modes have a positive dispersion relation, and the dispersion profiles of edge plasmon modes are similar to those found using local optical model by Xia and Quinn [14]. This again supports our identification of these edge plasmon modes.

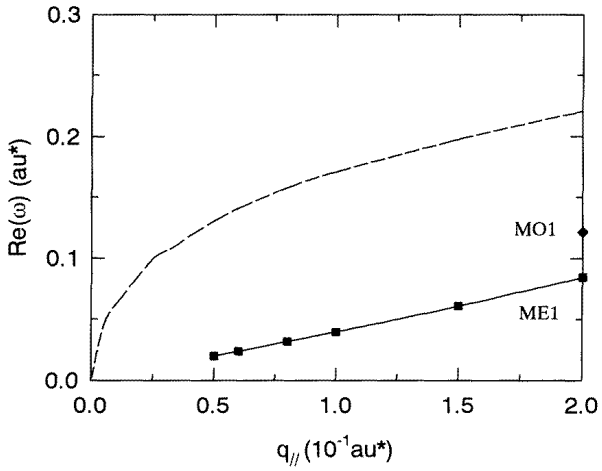

Figure 8. The dispersion relation Re(ω) versus $q_{\parallel}$ for the higher-multipole edge plasmon modes and the intrasubband plasmon mode (the dashed line) in the excitation spectra of PQW with width $L = 8.8$ au*, $n^+ = 0.0075$ au*.

3.2. The density dependence of edge plasmons

We now study the edge plasmon modes in PQW with width 8.8 au* and lower density $n^+ = 0.0075$ au*. The excitation spectrum with $q_{\parallel} = 0.10$ au* is shown in figure 6. Only one resonant mode ME1 located at the frequency 0.040 au* appears below the intrasubband plasmon. Calculation with the same well width and electron density but a larger $q_{\parallel}$ (0.20 au*) shows that another resonant mode MO1 appears at the frequency 0.121 au* in the excitation spectrum. The induced density profiles of these modes are presented in figure 7. It is easy to identify the resonant modes ME1 and MO1 as even and odd higher-multipole edge plasmon modes respectively. The dispersion profiles of the two edge plasmon modes are shown in figure 8. The system can support only one even edge plasmon mode for small values of $q_{\parallel}$. The corresponding odd edge plasmon mode appears at a larger wave vector $q_{\parallel} \cong 0.20$ au*. It is noted that the parabolic quantum well with higher electron density ($n^+ = 0.0275$ au*) can support more edge plasmon modes than the well with lower electron density ($n^+ = 0.0075$ au*). The dispersions of edge plasmon modes in both figure 5 and figure 8 show the interesting tendency that the even edge plasmon modes can be generated with small values of $q_{\parallel}$, whereas the corresponding odd edge plasmon modes can only be supported by the system for larger values of $q_{\parallel}$. This tendency may explain why the corresponding odd edge plasmon does not appear even at the large wave vector $q_{\parallel} = 0.20$ au* for PQW with $L = 8.8$ au* and $n^+ = 0.0275$ au*.

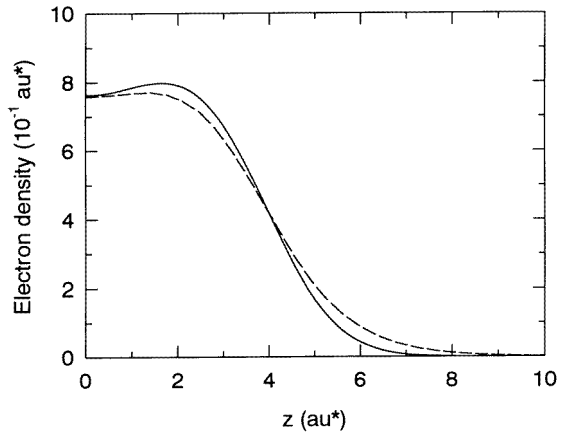

Figure 9. A comparison of the self-consistent edge electron distributions of PQW (the solid line) and NQW (the dashed line) with width $L = 8.8$ au* and density $n^+ = 0.0075$ au*.

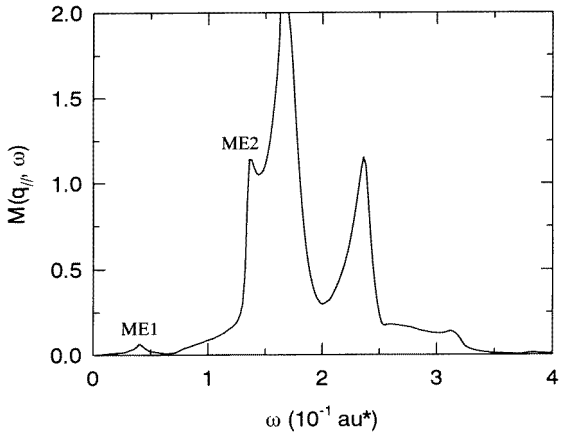

Figure 10. The excitation spectrum for NQW with width $L = 8.8$ au*, density $n^+ = 0.0075$ au*, $q_{\|} = 0.10$ au*, and $\mathrm{Im}(\omega) = 0.002$ au*.

3.3. The effect of the edge density on the edge plasmons

To investigate the effect of the edge electron distribution on the higher-multipole edge plasmon modes, we calculate the excitation modes in the neutral quantum well (NQW) with the same width L and fictitious density n^+ as those of the PQW studied in section 3.2. In figure 9, we compare the self-consistent electron distributions on the edges of PQW and NQW. The edge layer of electron density in NQW is much wider than that in PQW. The excitation spectrum with $q_{\|} = 0.10$ au* is shown in figure 10. It is interesting to note that a new even higher-multipole edge plasmon ME2 at $\omega = 0.137$ au* emerges below the intrasubband plasmon mode, in addition to the even higher-multipole edge plasmon ME1 at $\omega = 0.041$ au*, which have been observed in the PQW with the same conditions. This demonstrates that the edge electron distribution plays an important role in the appearance

of edge modes, and the values of $q_{\parallel}$ at which higher-multipole edge plasmon modes first appear become smaller as the edge electron distribution becomes wider.

4. Summary

In conclusion, we have studied the excitation modes in the parabolic quantum well via an approach based on the invariant-imbedding method. For large wave vectors, several weak resonant modes have been observed below the intrasubband plasmon mode and are identified as odd and even higher-multipole edge plasmon modes. It has been shown that the even edge plasmons can be generated by the system for small values of $q_{\parallel}$. However, the corresponding odd edge plasmons can only be supported for larger values of $q_{\parallel}$. There exist more edge plasmon modes in the PQW with higher-density electron gas than in the PQW with lower-density electron gas. Moreover, the edge electron distribution plays a key role in the appearance of edge higher-multipole plasma modes, and the values of $q_{\parallel}$ at which edge plasmon modes first appear become smaller as the edge electron distribution becomes wider. Further study of the dependence of edge plasmon modes on the edge density profiles is under way.

References

[1] Sundaram M, Gossard A C, English J H and Westervelt R M 1988 *Superlatt. Microstruct.* **4** 683
[2] Shayegan M, Sajoto T, Santos M and Silvestre C 1988 *Appl. Phys. Lett.* **53** 791
[3] Rimberg A J and Westervelt R M 1989 *Phys. Rev.* B **40** 3970
[4] Hopkins P F, Rimberg A J, Gwinn E G, Westervelt R M, Sundaram M and Gossard A C 1990 *Appl. Phys. Lett.* **57** 2823
[5] Pinsukanjana P R, Gwinn E G, Dobson J F, Yuh E L, Asmar N G, Sundaram M and Gossard A C 1992 *Phys. Rev.* B **46** 7284
[6] Kaloudis M, Ensslin K, Wixforth A, Sundaram M, English J H and Gossard A C 1992 *Phys. Rev.* B **46** 12 469
[7] Wixforth A, Sundaram M, Ensslin K, English J H and Gossard A C 1991 *Phys. Rev.* B **43** 10 000
[8] Liao L B Heiman D, Hopkins P F and Gossard A C 1994 *Phys. Rev.* B **49** 16 825
[9] Brey L, Johnson N F and Halperin B I 1989 *Phys. Rev.* B **40** 10 647
Brey L, Dempsey J, Johnson N F and Halperin B I 1990 *Phys. Rev.* B **42** 1240
[10] Guo Q, Poon H C, Feng Y P and Ong C K 1996 to be published
[11] Dobson J F 1992 *Phys. Rev.* B **46** 10 163
[12] Dobson J 1993 *Aust. J. Phys.* **46** 391
[13] Schaich W L and Dobson J F 1994 *Phys. Rev.* B **49** 14 700
[14] Xia X and Quinn J J 1994 *Phys. Rev.* B **50** 8032
[15] Burt M G 1992 *J. Phys.: Condens. Matter* **4** 6651
[16] Mahan D 1989 *Many Particle Physics* (New York: Plenum) p 405
[17] Mills D L 1975 *Surf. Sci.* **48** 59
[18] Zheng Lian, Schaich W L and MacDonald A H 1990 *Phys. Rev.* B **41** 8493
[19] Schaich W L, Park P W and MacDonald A H 1992 *Phys. Rev.* B **46** 12 643
[20] Adach S (ed) 1993 *Properties of Aluminium Gallium Arsenide* (London: Inspec)
[21] Kempa K, Liebsch A and Schaich W L 1988 *Phys. Rev.* B **38** 12 645
[22] Dobson J F and Harris G H 1988 *J. Phys. C: Solid State Phys.* **21** L729
Dobson J F, Harris G H and O'Connor A J 1990 *J. Phys.: Condens. Matter* **2** 6461
[23] Tsuei K-D, Plummer E W, Liebsch A, Kempa K and Bakshi P 1990 *Phys. Rev. Lett.* **64** 44
[24] Quinn J J 1992 *Solid State Commun.* **84** 139
[25] Mast D B, Dahm A J and Fetter A L 1985 *Phys. Rev. Lett.* **54** 1706
[26] Glattli D C, Andrei E Y, Deville G, Postrenaud J and Williams F I B 1985 *Phys. Rev. Lett.* **55** 879
[27] Wu J-W, Hawrylak P and Quinn J J 1985 *Phys. Rev. Lett.* **55** 876
[28] Wu J-W, Hawrylak P, Eliasson G and Quinn J J 1986 *Phys. Rev.* B **33**